Article

Solvent Friction Effect on Intramolecular Electron Transfer

Min Liu, Naoki Ito, Mark Maroncelli, David H. Waldeck, Anna M. Oliver, and Michael N. Paddon-Row

J. Am. Chem. Soc., **2005**, 127 (50), 17867-17876• DOI: 10.1021/ja055596a • Publication Date (Web): 25 November 2005

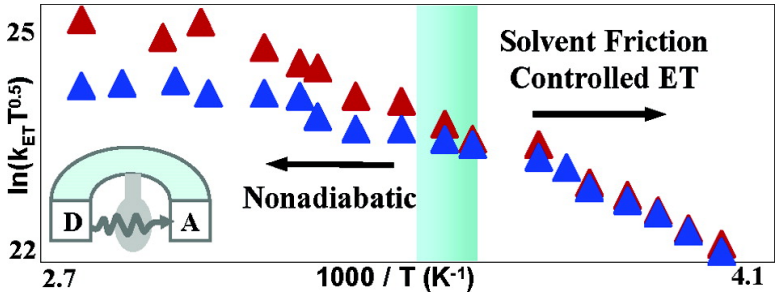

More About This Article

Additional resources and features associated with this article are available within the HTML version:

- Supporting Information
- Links to the 3 articles that cite this article, as of the time of this article download
- Access to high resolution figures
- Links to articles and content related to this article
- Copyright permission to reproduce figures and/or text from this article

View the Full Text HTML

J|A|C|S
ARTICLES
Published on Web 11/25/2005

Solvent Friction Effect on Intramolecular Electron Transfer

Min Liu,[‡] Naoki Ito,[†] Mark Maroncelli,*[,†] David H. Waldeck,*[,‡] Anna M. Oliver,[§] and Michael N. Paddon-Row*[,§]

Contribution from the Chemistry Department, University of Pittsburgh, Pittsburgh, Pennsylvania 15260, Department of Chemistry, Pennsylvania State University, University Park, Pennsylvania 16802, and School of Chemistry, University of New South Wales, Sydney NSW 2052, Australia

Received August 16, 2005; E-mail: dave@pitt.edu

Abstract: U-shaped donor−bridge−acceptor molecules with different electronic couplings have been investigated as a function of temperature in solvents with slow polarization relaxation, in particular, *N*-methylacetamide (NMA) and *N*-methylpropionamide (NMP). At high temperature, the electron-transfer rate is well described by a nonadiabatic model; however, the rate at low temperature is controlled by the solvent friction. The change of the electron-transfer mechanism is discussed and compared with theoretical models.

Introduction

Electron-transfer reactions are of broad importance in chemistry, biology, and related technologies. For this reason, a large body of work explores electron-transfer processes over a broad range of different conditions and systems.[1−4] Our work addresses fundamental issues in electron transfer by using donor−bridge−acceptor molecules to manipulate the interaction between the electron donor (reductant) and electron acceptor (oxidant) groups. The present work reports studies of two different donor−bridge−acceptor molecules in polar solvents with different solvation time scales and demonstrates how electron transfer proceeds from electron tunneling control to solvent friction control.

Most studies have found that electron-transfer reactions proceed in one of a few limiting regimes: nonadiabatic electron transfer, adiabatic electron transfer, or solvent-controlled electron transfer. In nonadiabatic electron-transfer reactions, the reaction rate constant is appropriately described by a transition state theory rate constant times a transmission factor which depends on the electron tunneling probability. In the adiabatic and solvent-controlled electron-transfer regimes, the reaction rate is controlled by nuclear motion(s) of the system through the transition state region, rather than by the electron tunneling probability. The current studies are distinguished from other works by the ability to probe how the electron-transfer rate constant proceeds from a nonadiabatic mechanism to a solvent-controlled mechanism.

A previous study considered photoinduced intramolecular electron transfer in two U-shaped donor−bridge−acceptor molecules **1** and **2** (see Scheme 1). Upon photoexcitation, these molecules transfer an electron from the naphthalenic group to the dicyanovinyl group by electron tunneling through the imide-functionalized cleft.[5] The nature of the chemical group (pendant) in the cleft changes the electron tunneling probability. An earlier study[6] demonstrated the transition between nonadiabatic (electron tunneling) electron transfer and solvent-controlled electron transfer in the system **1**, by comparing the rate constant in acetonitrile to that in *N*-methylacetamide. The current work extends that study by varying the initial excitation energy of the donor, by performing rate studies in *N*-methylpropionamide, which has dielectric properties similar to those of NMA but remains a liquid over the entire temperature range, and by measuring the solvent polarization relaxation times of these solvents, which allows quantitative comparisons of the rate constant behavior with model predictions.

This report has five major sections. The next section provides background on electron-transfer models that account for solvent frictional coupling and briefly describes solvation models. The following section describes the experimental details. The next two sections analyze the experimental results and compare them to the models. The last section concludes this work and describes its implications.

Background

For the U-shaped molecules investigated here, the electronic coupling between the donor and acceptor groups is weak enough that a nonadiabatic picture applies. Previous work[5] showed that

[†] University of Pittsburgh.
[‡] Pennsylvania State University.
[§] University of New South Wales.

(1) Barbara, P. F.; Meyer, T. J.; Ratner, M. A. *J. Phys. Chem.* **1996**, *100*, 13148.
(2) Zimmt, M. B.; Waldeck, D. H. *J. Phys. Chem. A* **2003**, *107*, 3580.
(3) Jortner, J. *Advances In Chemical Physics: Electron Transfer From Isolated Molecules*, series #2; Wiley: New York, 1999; Vol. 107.
(4) Sumi, H. In *Adiabatic versus Non-Adiabatic Electron Transfer in Electron Transfer in Chemistry*; Balzani, V., Ed.; Wiley: New York, 2001; Vol. 1, Chapter 2, pp 65−108.
(5) (a) Napper, A. M.; Head, N. J.; Oliver, A. M.; Shephard, M. J.; Paddon-Row, M. N.; Read, I.; Waldeck, D. H. *J. Am. Chem. Soc.* **2002**, *124*, 10171. (b) Napper, A. M.; Read, I.; Waldeck, D. H.; Head, N. J.; Oliver, A. M.; Paddon-Row, M. N. *J. Am. Chem. Soc.* **2000**, *122*, 5220.
(6) Liu, M.; Waldeck, D. H.; Oliver, A. M.; Head, N. J.; Paddon-Row, M. N. *J. Am. Chem. Soc.* **2004**, *126*, 10778.

Scheme 1

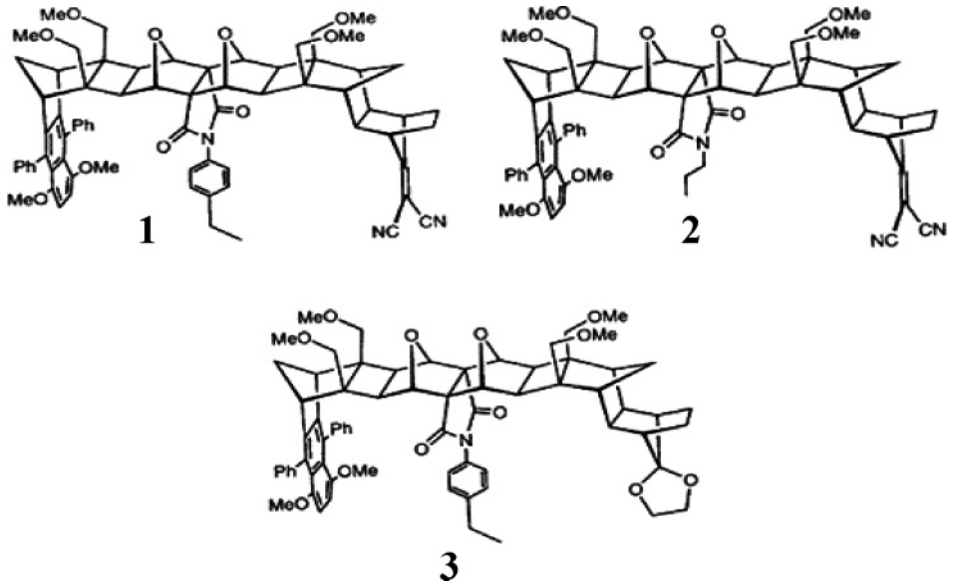

the Golden Rule rate constant expression k_{NA}[7] with a single effective quantum mode

$$k_{NA} = \frac{4\pi^2}{h}|V|^2 \frac{1}{\sqrt{4\lambda_0 \pi k_B T}} \sum_{n=0}^{\infty} \exp(-S)\left(\frac{S^n}{n!}\right) \exp\left[-\frac{(\Delta_r G + \lambda_0 + nh\nu)^2}{4\lambda_0 k_B T}\right] \quad (1)$$

adequately describes the rate behavior in simple solvents with rapid dielectric relaxation times. In eq 1, λ_0 is the solvent reorganization energy; $\Delta_r G$ is reaction free energy; λ_v is the energy required for high-frequency vibrational reorganization; $|V|$ is the electronic coupling between the reactant and the product states, and $S = \lambda_v/h\nu$. The $h\nu$ term is the energy spacing of a single effective quantized vibration associated with the electron-transfer event, which is taken to be a characteristic feature of the solute. The sum is performed over the vibrational states of the effective quantum mode. The semiclassical theory treats the low-frequency modes classically. The electronic coupling $|V|$ in the U-shaped molecules studied here is smaller than $k_B T$, but not much smaller, and it is possible to observe a change in electron-transfer mechanism by changing the solvent friction.

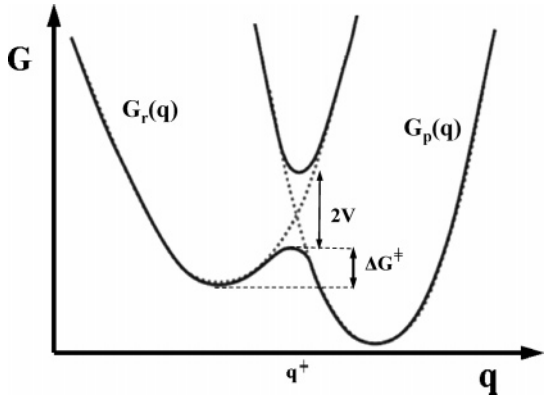

Figure 1. Diagram illustrating the adiabatic and nonadiabatic potential surfaces; for adiabatic electron transfer (strong coupling), the solid curves apply, whereas for nonadiabatic electron transfer, the diabatic (dashed) curves apply (**r** denotes the reactant and **p** denotes the product).

Three different regimes, or mechanisms, are observed in electron-transfer reactions: nonadiabatic electron transfer, adiabatic electron transfer, and solvent-controlled electron transfer. In the nonadiabatic case, the electronic coupling is weak, $|V| \ll k_B T$, the rate constant is proportional to $|V|^2$ and eq 1 applies. In this limit, the system may move through the curve-crossing region $\mathbf{q}^{\ddagger}$ many times before the electronic state changes from **r** to **p** (see Figure 1). In the adiabatic case, $|V| \gg k_B T$, and the reaction proceeds by nuclear motion through the transition state along a single electronic surface. The effect of $|V|$ on the rate constant is only manifest through its role in determining the energy barrier, $\Delta G^{\ddagger}$ (Figure 1). In the solvent-controlled limit, the electronic coupling may still be small; however, the rate constant is affected by frictional coupling. In this case, the characteristic time spent in the curve-crossing region is long enough that the electronic state changes from **r** to **p** for nearly every approach, even though the coupling is weak. Hence the reaction appears to be adiabatic in the sense that the rate is limited by nuclear dynamics rather than by the electron tunneling probability.

Zusman[8] generalized the rate constant expression for electron-transfer k_{ET} to describe a transition between the normal nonadiabatic limit, k_{NA}, and a solvent-controlled limit, k_{SC}, namely

$$\frac{1}{k_{ET}} = \frac{1}{k_{SC}} + \frac{1}{k_{NA}} \quad (2)$$

Equation 2 shows that the measured electron-transfer rate k_{ET} can be limited by either the electronic motion (k_{NA} is small) or the nuclear motion (k_{SC} is small). The slower process is rate controlling. In the classical limit he found

$$k_{SC} = \frac{1}{\tau_s}\frac{\lambda_0}{\pi^3 k_B T} \sin\left(\pi \frac{\Delta G^{\ddagger}}{\lambda_0}\right) \exp\left(-\Delta G^{\ddagger} k_B T\right) \quad (3)$$

in which the electron-transfer rate is proportional to the solvation

(7) Jortner, J. *J. Chem. Phys.* **1976**, *64*, 4860.
(8) (a) Zusman, L. D. *Chem. Phys.* **1980**, *49*, 295. (b) Zusman, L. D. *Chem. Phys.* **1983**, *80*, 29. (c) Zusman, L. D. *Z. Phys. Chem.* **1994**, *186*, 1.

rate, $1/\tau_s$. Since the solvation time τ_s increases dramatically with decreasing temperature, especially in viscous solvents, the solvation time becomes more important as the temperature is lowered.

Sumi and Marcus[9] considered the combined effects of intramolecular vibrations and diffusive solvent orientational motions on electron transfer. They described the reaction as proceeding along a two-dimensional effective potential energy surface, $V(q,X)$. The coordinate X corresponds to the solvent polarization (the polarization response of the solvent to changes of the charge distribution), and q is an intramolecular vibrational coordinate, which includes the fast nuclear motions typical of electron-transfer reactions in the nonadiabatic or adiabatic limit. To find the reaction rate, they solved the Fokker−Planck equation for diffusive motion along X and treated the motion along q through a rate constant $k(X)$ that depends on the "fast" motions in the normal way (e.g., eq 1) and depends parametrically on X.[6,9] More detail on this model is provided in the Data Analysis section as it is needed and in the Supporting Information.

Previous modeling[5] of these U-shaped molecules in fast solvents found an internal reorganization energy λ_ν of 0.65 eV and an effective quantum mode frequency of 1600 cm^{-1}. Comparison with solvation models indicates that the solvent reorganization energy λ_0 lies between 1.2 and 1.4 eV for **1** and **2** in NMA and NMP (vide infra). The ratio λ_ν/λ_0 is thus approximately 0.5, which places these reactions in the narrow reaction window limit of Sumi and Marcus.[6,9] This limit is also one in which Zusman's predictions (eqs 2 and 3) should apply. Sumi and Marcus pointed out the nonexponential character in the narrow reaction window limit; however, Zusman's treatment does not address this feature.

Solvation: The solvent reorganization energy and reaction free energy are important determinants of the electron-transfer rate in any of the limits, and accurately modeling these solvation energies as a function of temperature is important to properly interpreting the present experiments. Two models are currently popular for describing solvation energies— the dielectric continuum model and a molecular solvation model. The dielectric continuum model[10] calculates solvation energies using the static dielectric constant ϵ_s and a high-frequency dielectric constant ϵ_∞ of the solvent. In its simplest implementation, the solute is treated as a spherical (or ellipsoidal) cavity containing a point dipole. The solvent reorganization energy is described as

$$\lambda_0 = \frac{(\Delta\mu)^2}{{a_0}^3}\left(\frac{\epsilon_s - 1}{2\epsilon_s + 1} - \frac{\epsilon_\infty - 1}{2\epsilon_\infty + 1}\right) \quad (4)$$

and the reaction free energy from this model is

$$\Delta_r G = \Delta_{vac} G - \frac{(\mu_{CS}^2 - \mu_{LE}^2)}{{a_0}^3}\left(\frac{\epsilon_s - 1}{2\epsilon_s + 1}\right) \quad (5)$$

where μ_{LE} is the dipole moment of the initially excited state, μ_{CS} is the dipole moment of the charge-separated state, and a_0 is the cavity radius. $\Delta\mu$ is the magnitude of the dipole moment difference vector between the locally excited and the charge-separated states; that is, $\Delta\mu \equiv |\vec{\mu}_{CS} - \vec{\mu}_{LE}|$. $\Delta_{vac}G$ is the reaction Gibbs free energy in the absence of solvation.

The molecular solvation model developed by Matyushov[11] accounts for the discrete nature of the solute and the solvent. Typically, the solute is approximated by a sphere with a point dipole moment and polarizability, and the solvent is modeled as a polarizable sphere, with an electrostatic charge distribution that includes both a point dipole and a point quadrupole. The molecular solvation model is more realistic than the dielectric continuum model because it includes not only the dipole−dipole interactions but also the dipole−quadrupole interactions between the solute and solvent. Importantly, the molecular model properly accounts for the temperature dependence of the solvation.[12]

Previous reports[5] parametrized the molecular solvation model for **1** and **2** in the weakly polar solvents toluene and mesitylene. In that work, excited-state equilibria between the charge-separated state and the locally excited state were used to calibrate the molecular solvation model for the reaction free energy. This parametrization was shown to provide temperature-dependent reorganization energies in good accord with experiment. In the present work, the molecular solvation model and these previously derived model parameters are utilized to calculate the reaction free energies and solvent reorganization energies of **1** and **2**. The new features in the parametrization are those for the NMA and NMP solvent molecules (vide infra). This procedure provides a self-consistent analysis for these solute molecules.

Experimental Section

The structures of **1**, **2**, and **3** are shown in Scheme 1. Synthesis of the U-shaped supermolecules is reported elsewhere.[13] The solvent *N*-methylacetamide (NMA) was purchased from Aldrich, and *N*-methylpropionamide (NMP) was purchased from TCI America. NMA and NMP were fractionally distilled three times using a vigreux column under vacuum. The freshly purified fraction was used in all the experiments. Each sample went through a freeze−pump−thaw procedure five or more times to eliminate dissolved oxygen.

Time-resolved fluorescence kinetics of **1** and **2** were measured using the time-correlated single photon counting technique.[14] The instrument used here is based on the frequency-doubled output of a cavity-dumped Coherent CR599-01 dye laser, which was pumped by a mode-locked Coherent Antares Nd:YAG laser. The full-width at half-maximum of the instrument function is ~60 ps. Different dyes were used in this experiment to obtain the different excitation wavelengths: Rhodamine 6G dye was used to obtain 296 and 310 nm wavelength; DCM dye was used to obtain 326 nm; and LDS 722 (also named pyridine 2 dye) was used to obtain 359 nm wavelength. The dye laser pulse train had a repetition rate of ca. 300 kHz. Pulse energies were kept below 1 nJ, and the count rates were kept below 3 kHz to prevent pile-up effects. All fluorescence measurements were made at the magic angle, and data were collected until a standard maximum count of 10 000 was observed at one channel.

(9) Sumi, H.; Marcus, R. A. *J. Chem. Phys.* **1986**, *84*, 4894.
(10) (a) Newton, M. D.; Basilevsky, M. V.; Rostov, I. V. *Chem. Phys.* **1998**, *232*, 201. (b) Sharp, K. A.; Honig, B. *Annu. Rev. Biophys. Chem.* **1990**, *19*, 301. (c) Sitkoff, D.; Sharp, K. A.; Honig, B. *J. Phys. Chem.* **1994**, *98*, 1978. (d) Brunschwig, B. S.; Ehrenson, S.; Sutin, N. *J. Phys. Chem.* **1986**, *90*, 3657.
(11) (a) Matyushov, D. V.; Voth, G. A. *J. Chem. Phys.* **1999**, *111*, 3630. (b) Matyushov, D. V. *Chem. Phys.* **1993**, *174*, 199. (c) Matyushov, D. V. *Mol. Phys.* **1993**, *79*, 795.
(12) Vath, P.; Zimmt, M. B.; Matyushov, D. V.; Voth, G. A. *J. Phys. Chem. B* **1999**, *103*, 9130.
(13) (a) Head, N. J.; Oliver, A. M.; Look, K.; Lokan, N. R.; Jones, G. A.; Paddon-Row, M. N. *Angew. Chem., Int. Ed.* **1999**, *38*, 3219. (b) Supporting Information of ref 6a.
(14) O'Connor, D. V.; Phillips, D. *Time-Correlated Single Photon Counting*; Academic Press: London, Orlando, 1984.

The experiments for **1**, **2**, and their donor-only analogues were carried out in NMA and NMP as functions of temperature at four different excitation energies. The temperature ranged from a low of 226 K to a high of 353 K. At the high end of this range, temperatures were controlled by an ENDOCAL RTE-4 chiller, measured using a type-K thermocouple (Fisher-Scientific), accurate to within 0.1 °C. Measurements at lower temperatures employed a VPF-100 Cryostat (Janis Research Company, Inc.) and a Model 321 Autotuning Temperature Controller (LakeShore Cryotronics, Inc.) with a silicon diode sensor. The low-temperature instrumental setup is shown in the Supporting Information.

Temperature measurement was improved from the earlier design by including another type-T thermocouple attached on the surface of the cuvette to monitor the temperature, in addition to the silicon sensor used for temperature control, which is not directly in contact with the sample cuvette. The temperatures measured at the cuvette surface are close to those measured when a thermocouple is directly inserted into the liquid sample, within 1 K, but they are systematically higher than the temperature measured from the diode sensor. The worst case was observed at the lowest temperature (220 K) which has a 10 K difference.

Lifetime Measurements: The samples of **1** and **2** each contain a small amount of unreacted donor compound. Independent experiments on the donor-only molecule **3** were used to characterize its single-exponential fluorescence decay, which is much longer than the relaxation times of **1** and **2** at the measurement temperatures. To account for emission from this impurity, a component with the lifetime of the donor-only molecule **3** was fixed in the fits to the data collected with compounds **1** and **2**. The impurity component amounted to less than 8% of the overall decay law in all cases. The remaining parts of the **1** and **2** decay laws in NMA and NMP were fit as a double-exponential functions using IBH-DAS6 analysis software. The instrument response function, measured using a sample of colloidal $BaSO_4$, was convoluted with the decay curves.

Time-Resolved Stokes Shift Measurements: For solvation measurements, samples at concentrations providing optical densities of ~0.1 for a 1 cm path length were prepared in quartz cuvettes. Samples above 7 °C were thermostated to ±0.1 °C using a circulating water bath and sample holder assembly. For lower-temperature measurements, sealed cryogenic cuvettes were enclosed in a copper block mounted on the coldfinger of a liquid nitrogen cryostat (Oxford Instruments DN1754). With this system, temperatures between 85 and 300 K could be maintained constant to within ~1 K.

Time-resolved emission measurements were made using a time-correlated single-photon counting system previously described.[15] This system employed the doubled output of a femtosecond mode-locked Ti:sapphire laser (Coherent Mira 900F) for excitation at 420 or 374 nm and had an overall response time of 25 ps (fwhm) for higher temperatures and 100 ps for lower temperatures using the cryostat, as measured by scattering. The repetition rate of the excitation was set according to the lifetime of the solvation probe. Emission was collected through a single monochromator (ISA H10) with a 4 nm band-pass. Emission decays were fit with instrumental response functions using an iterative reconvolution least-squares algorithm,[16] which enhances the effective time resolution to ~5 ps. Time-resolved emission spectra were constructed from a series of nine to twelve magic angle decays recorded at wavelengths spanning the emission spectrum, as previously described.[17]

Steady-state emission spectra were measured on a Spex Fluorolog 1680 (0.22 m double spectrometer with 1 s integration time). The steady-state spectra were utilized to normalize the time-resolved emission spectra at each temperature.

(15) Heitz, M. P.; Maroncelli, M. *J. Phys. Chem. A* **1997**, *101*, 5852.
(16) Birch, D. J. S.; Imhof, R. E. In *Topics in Fluorescence Spectroscopy: Techniques*; Lakowicz, J. R., Ed.; Plenum: New York, 1991; Vol. 1, pp 1−95.
(17) Maroncelli, M.; Fleming, G. R. *J. Chem. Phys.* **1987**, *86*, 6221.

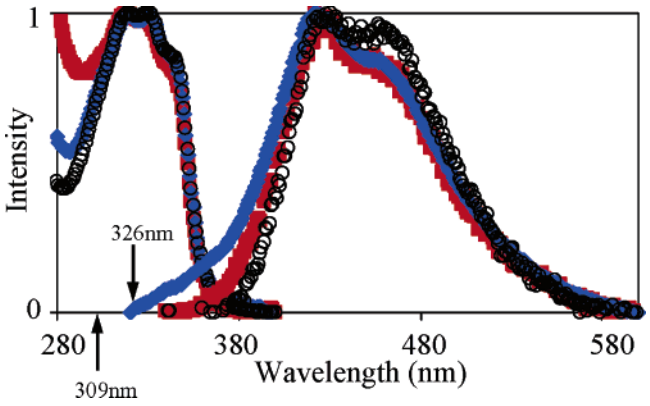

Figure 2. Steady-state spectra of **1** in ACN (black circle), NMA (red square), and NMP (blue diamond). The absorption spectra are on the left, and the emission spectra are on the right.

Table 1. Properties of ACN, NMA, and NMP Solvents at 303 K

solvent	refractive index[a]	static dielectric constant[a]	Debye relaxation time[18] (ps)	average solvation time (ps)	viscosity[a] (cP)	dipole moment (D)
ACN	1.34	34.75	3	0.9	0.3	3.48
NMA	1.43	178.9	390	35[b]	3.9	5.05[c]
NMP	1.43	164.4	100	42[b]	4.6	4.29[c]

[a] Beilstein database. [b] Extracted from the best fit of the dynamic Stokes shift measurements. [c] Calculated using Gaussian/MP2/6-31G.

Results

Steady-State Spectra: Steady-state spectra of **1** in three different solvents (acetonitrile, ACN; *N*-methylacetamide, NMA; *N*-methylpropionamide, NMP) are compared in Figure 2. It is evident that the spectral shapes are very similar in these three solvents, which suggests that the solvent molecules do not alter the spectroscopic characteristics of the donor group; that is, the three solvents interact similarly with the solute. The higher emission of **1** in NMP between 340 and 360 nm arises from an impurity in NMP. Lifetime measurements were carried out at longer wavelengths to avoid interference from this solvent impurity emission.

The solvents ACN, NMA, and NMP have very different solvation dynamics. Table 1 reports some properties of these solvents at 303 K. ACN has very fast relaxation times and low viscosity, so it can reorient much faster than the measured electron-transfer rate. As for NMA and NMP, the slow relaxation times mean that polarization fluctuations occur on time scales that are similar to, or slower than, the electron-transfer time scale.

Solvent Comparisons: The intramolecular electron transfer in **1** and **2** occurs from the locally excited state of the dimethoxydiphenylnaphthalene donor to generate a nonfluorescent charge-separated state. Because the electron transfer competes with the intrinsic fluorescence, the change in the fluorescence decay law with solvent or temperature directly reflects the change in the electron-transfer rate. By assuming that the excited-state decay law without electron transfer can be determined by measuring the decay law of the donor-only compound, k_F (**3**), the electron-transfer rate constant k_{ET} can be found from the difference of the measured fluorescence rate constants k_F; that is, $k_{ET} = k_F - k_F$ (**3**). Fluorescence lifetime experiments were performed at different temperatures ranging

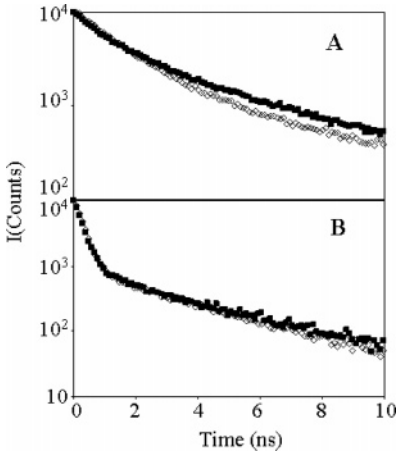

Figure 3. The decay curves of **1** in NMA (filled black square) and NMP (opened gray diamond) at 250 K (A) and 333 K (B) excited at 326 nm.

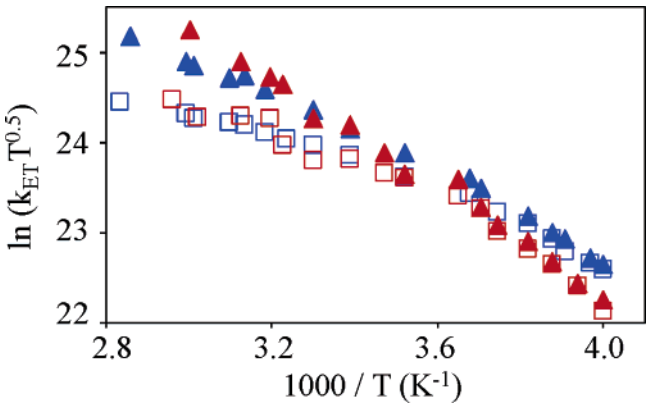

Figure 4. Electron-transfer rate constants of **1** (filled triangle) and **2** (opened square) in NMP (blue) and NMA (red) as a function of temperature excited at 309 nm. The format of this plot is such that the data should be linear if eq 1 is obeyed.

from 360 to 226 K, in the different solvents NMA, NMP, and ACN, and at different excitation energies (296, 309, 326, and 359 nm).

Similar to the results reported earlier in NMA, the fluorescence decay of **1** in NMP is nonexponential at low temperature and becomes more exponential at higher temperatures. At 232 K, a fast lifetime component of 1.96 ns with an amplitude of 52% is observed. With increasing temperature, the amplitude of the fast component increases, and the overall decay law becomes more like a single-exponential function. For example, a fast component of 224 ps with a 94% amplitude ratio is observed at 333 K.

Because the decay law is not single exponential, the electron-transfer rate constant is not well-defined. To quantify the rate in terms of an effective rate constant, a correlation time τ_c is computed from the fluorescence decay law, namely, $\tau_c = f_1\tau_1 + (1 - f_1)\tau_2$. Here, τ_1 and τ_2 are the two time constants obtained from the decay fits, and f_1 is the fractional amplitude of the short time constant, excluding the contribution from the donor-only impurity. By subtracting the donor-only lifetime, an effective electron-transfer rate constant is found, $k_{ET} = 1/\tau_c - k(\mathbf{3})$. This choice goes smoothly to the proper rate constant as the decay law becomes single exponential.

To compare the behavior in NMA and NMP, the decay curves of **1** in NMA and NMP at two representative temperatures are plotted in Figure 3. Note that the donor-only impurity has been removed from these data. The difference between the decay curves at 333 K is small. At high temperature, the static dielectric properties of NMA and NMP are similar. If the solvation in the two solvents are similar ($\Delta_r G$ and λ), then the nonadiabatic electron-transfer rate of **1** in these solvents should be similar, as observed. Note that the second component in the decay law in Figure 3B is only ~3% in amplitude. At 250 K, the two decay curves differ more than at high temperature.

To better illustrate the differences between electron transfer in NMA and NMP, the temperature dependence of the experimental rate constants is plotted in Figure 4. For a given solute−solvent combination, this plot should be linear if the semiclassical equation for nonadiabatic electron transfer (eq 1) is followed, which is supported by the rate data for both **1** and **2** in each solvent at high temperature. The temperature dependence of the rate constants of **1** and **2** in NMP is qualitatively similar to that observed in NMA. As the temperature increases, the electron-transfer rates of **1** and **2** in NMP become more different, but with decreasing temperature, they become more alike. At high temperature, the rate constant of **1** is similar in NMA and NMP (also for **2**), and differences in the solvent are less important. In contrast, the rate constants at low temperature are separated by the solvent type rather than the solute type.

An earlier report[6] compared the electron-transfer rate constants in NMA to those in acetonitrile and showed that for acetonitrile the rate constants of **1** and **2** remained displaced over the entire temperature range. Hence the change in character of the k_{ET} versus T plot observed here results from properties of the solvents, not just the temperature.

Both NMP and NMA are highly polar and have "very slow" dielectric relaxation times (see Table 1). At high temperatures, the electron-transfer rates of **1** and **2** in NMA and NMP are very similar, suggesting that the reorganization and reaction free energies are similar, a result which is consistent with the large dielectric constants of these solvents and a nonadiabatic electron-transfer mechanism. At low temperatures, the electron transfer appears to be controlled by the solvent, and they are different in NMA and NMP. Considering their different physical properties (NMA solidifies at temperatures below 303 K, whereas NMP remains a liquid even at 226 K; see below), it is reasonable to expect that the solvation time of NMA is longer than that of NMP, and that the viscosity of NMA is higher than that of NMP. If the solvent dynamics controls the electron-transfer rate, then one expects a smaller rate constant for NMA, as observed.

Excitation Energy: If the solvent is sluggish enough, then the locally excited state may not be equilibrated with the solvent before electron transfer. To test for this nonequilibrium effect on the reaction, the fluorescence decay was studied as a function of excitation energy. Figure 5 shows the temperature dependence of the rate constants for **1** and **2** at two different excitation energies, 309 and 326 nm. Another excitation wavelength 296 nm was also studied, and its rate is not distinguishable from that of 309 and 326 nm. Experiments, using 359 nm excitation were not conclusive because of weak signal levels.

As illustrated in Figure 5, the electron-transfer rates for **1** and **2** do not vary significantly with the excitation energy. This behavior is consistent with electron transfer from a locally excited state that is equilibrated with the solvent; that is, even though the solute is excited with a higher energy, the solute molecules retain no memory of the initial excess energy. In the

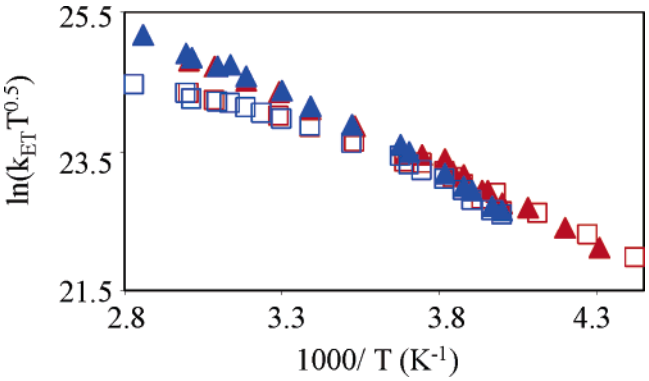

Figure 5. Electron-transfer rates of **1** (filled triangle) and **2** (opened square) in NMP at different temperatures excited at 309 nm (blue) and 326 nm (red).

subsequent analysis, we therefore focus exclusively on data collected using 309 nm excitation.

Dynamic Stokes Shift: To better quantify how the solvent dynamics affects the electron transfer, dynamic Stokes shift measurements of solvation times were performed in NMA and NMP. Because the Stokes shifts of **1** and **2** are small, other solute chromophores were used to probe the solvent response. In NMP, the solute 4-aminophthalimide was used to measure the solvation time. For temperatures ranging from 240 to 298 K, the solvation time varies from 719 to 56 ps. Because the relaxation in NMA is so slow, two solutes were used: $Ru(bpy)_2(CN)_2$ at 200 K and 4-aminophthalimide at temperatures ranging from 220 to 298 K. For $Ru(bpy)_2(CN)_2$ in NMA, the solvation time is approximately 560 ns at 200 K, and for 4-aminophthalimide in NMA, the solvation time varies from 32 ns at 220 K to 70 ps at 298 K.

Figure 6 compares the solvation times measured in NMA and NMP as functions of temperature. The time-dependent Stokes shift measurements indicate that the solvation times of NMA and NMP are similar at high temperature and become more dissimilar as the temperature decreases. This behavior is consistent with their effect on the electron transfer. It is also evident that solvation in NMA and NMP is slower than the electron-transfer rate of **1** and **2** at low temperatures. For example, in NMA at 220 K, the solvation time is 32 ns, whereas the time constant for electron transfer in both solutes is ~3 ns. The slower the solvation time, the slower are the polarization fluctuations, which can lead to a solvent friction dependence of the electron-transfer rates.

Data Analysis

High-Temperature Analysis: At temperatures between 360 and 295 K, the rate laws for **1** and **2** in NMA and NMP are nearly exponential. For example, for **1** in NMP at 334 K, the midpoint of this range, the fast decay time is 231 ps with an amplitude of 94%, whereas the correlation time is 259 ps, an 11% difference. The worst case is the decay time at 295 K for which the correlation time is 504 ps and the fast decay time is 427 ps, a 15% difference. As the temperature increases, the correspondence between the correlation time and the fast decay component improves. The molecule **2** in NMA and NMP approximates a single-exponential decay law even better than **1**. This latter finding is consistent with the weaker electronic coupling between the donor and acceptor groups in **2**, as compared to that of **1**.

Previous studies applied eq 1 to fit the experimental rate constant of **1** and **2** as functions of temperature and extracted values of the electronic coupling $|V|$ for the two systems. At high temperatures, where the decay rate constants of **1** and **2** in NMA and NMP appear to be controlled by the solute molecular properties and the solvents' static dielectric properties, the same analysis can be applied. Both experimental[2] and theoretical[19] work show that the electronic coupling can be modified by the solvent; however, previous work demonstrates that such affects are minor for these compounds.[5,6,20]

Figure 7 shows a fit to these high-temperature data with eq 1. For comparison purposes, Figure 7 includes earlier data for **1** and **2** in acetonitrile with the new data in NMA and NMP at high temperatures (>300 K). The data are fit to eq 1 and calibrated to the measured free energies in nonpolar solvents as described in ref 21. The molecular solvation model employed in these fits requires several solvent parameters, which are specified in ref 22. The values of the electronic coupling $|V|$, λ_v, and $h\nu$ were the same as determined from the previous work,[6] and $\Delta_r G$ and λ_0 were predicted using the calibrated Matyushov

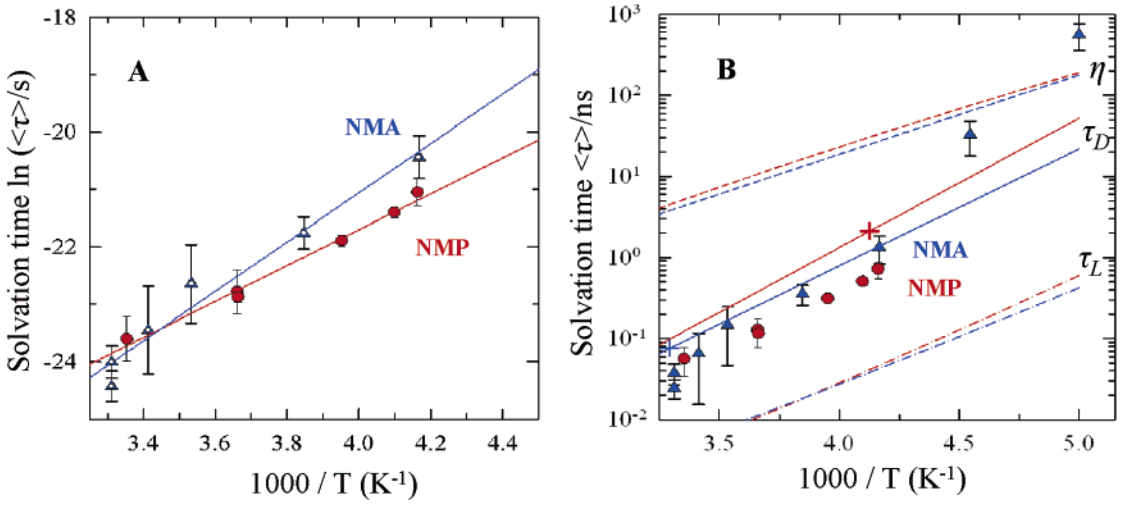

Figure 6. The experimental solvation times of NMA (blue triangle) and NMP (red circle) are plotted as a function of temperature. The curves in panel A are the best fit of the data points. Panel B compares the solvation times for NMA and NMP to the viscosity η, the Debye relaxation time τ_D, and the longitudinal dielectric relaxation time τ_L for the solvents (NMA is blue, NMP is red) from literature data (see Supporting Information for details).

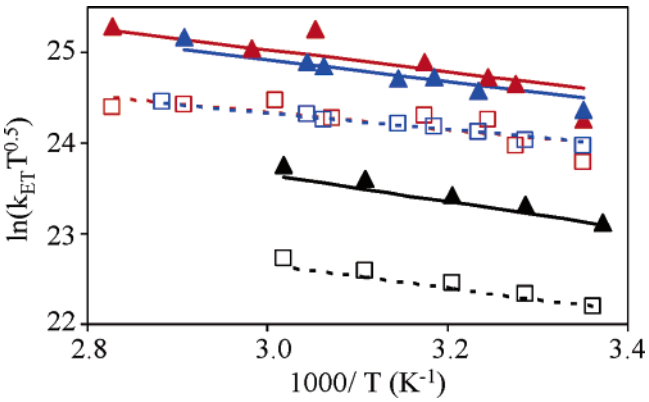

Figure 7. Electron-transfer rate constants of **1** (filled triangle) and **2** (opened square) in ACN (black), NMA (red), and NMP (blue) excited at 309 nm. The lines represent fits to eq 1.

Table 2. Fitting Parameters for **1** and **2** to the Nonadiabatic Model at High Temperature[a]

		CH_3CN (295 °C)		NMA (303 °C)		NMP (295 °C)	
system	$\|V\|$ (cm^{-1})	λ_0(eV)	Δ_rG (eV)	λ_0 (eV)	Δ_rG (eV)	λ_0 (eV)	Δ_rG (eV)
1	146	1.49	−0.54	1.36	−0.56	1.32	−0.52
2	62	1.46	−0.58	1.28	−0.61	1.23	−0.57

[a] Values of λ_v= 0.63 eV and $h\nu$ = 1600 cm^{-1} are determined from charge-transfer spectra of related species.

model. The experimental electron-transfer rate constant for **1** is faster than that for **2** in these solvents, which matches well with the previous conclusion that the aromatic group is better than an alkyl group at mediating the electronic coupling. The fitting parameters for **1** and **2** in NMA and NMP are listed in Table 2. Figure 7 also reveals that the electron-transfer rate for both **1** and **2** in the slow solvents NMA and NMP is higher than the rate in acetonitrile. Since the electronic coupling of **1** and **2** is assumed to be solvent independent, the difference of the rate constants in NMA and NMP with those in acetonitrile is understood as reflecting differences in the activation energies in these solvents, $\Delta G^{\ddagger} \sim (\Delta_rG + \lambda)^2/4\lambda$.

Low-Temperature Analysis: The semiclassical equation (eq 1) does not describe the electron-transfer dynamics in the low-temperature limit because it does not account for solvent frictional effects. Figure 8 compares the low-temperature predictions of eq 1 using parameters obtained from the high-

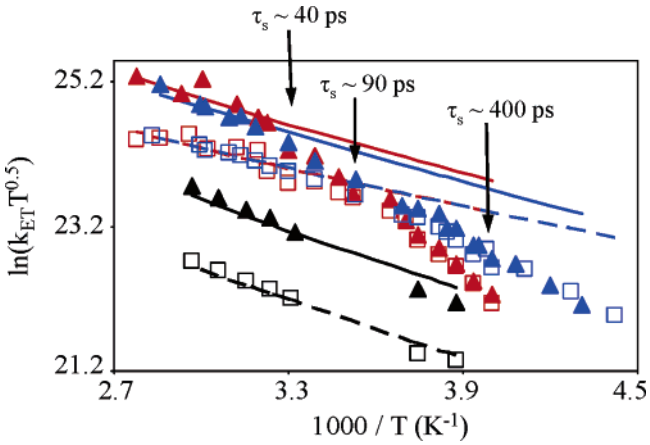

Figure 8. Electron-transfer rate constants of **1** (filled triangle) and **2** (opened square) in acetonitrile (black), NMA (red), and NMP (blue) excited at 309 nm. The lines represent fits to eq 1.

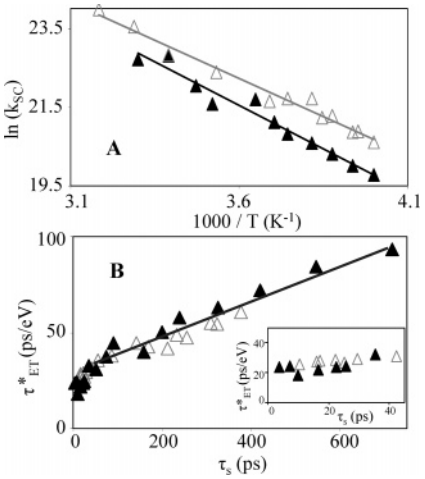

Figure 9. (A) Electron-transfer rate constant of **1** in NMA (filled black triangle) and NMP (opened gray triangle) in the solvent friction region. (B) Interpolation τ^*_{ET} of **1** in NMA (filled black triangle) and NMP (opened gray triangle) versus solvation time; the straight line is a linear fit. The insert expands the region $0 \le \tau_s(ps) \le 40$ for clarity.

temperature fit in Figure 7. In the case of acetonitrile, the nonadiabatic expression (eq 1) provides a good description of the rate constant over the whole temperature range studied. In contrast, in the slower solvents NMA and NMP, the observed low-temperature rates fall well below those extrapolated from the high-temperature fits.

Assuming that the rate constant is a serial combination of nonadiabatic and solvent-controlled rate constants as in eq 2, the solvent-controlled rate constant k_{SC} can be obtained from the experimental value k_{ET} and the extrapolated nonadiabatic value k_{NA}; that is, from eq 2. Figure 9A plots the solvent-controlled rate constant for **1** in NMA and NMP as a function of 1000/*T*. The rate constant increases with temperature, and the activation energy is similar for the two solvents, 37 kJ/mol for NMA and 32 kJ/mol for NMP.

Zusman Model: According to Zusman,[8] the electron-transfer rate constant is inversely proportional to the solvation time when the reaction proceeds in the solvent friction regime, but it becomes independent of solvent friction when the solvation time is rapid. The Zusman treatment uses the interpolation formula (eq 2). Comparison to this model is facilitated by defining the quantity τ^*_{ET} as

(18) Maroncelli, M. *J. Mol. Liq.* **1993**, *57*, 1.
(19) (a) Hsu, C.-P.; Fleming, G. R.; Head-Gordon, M.; Head-Gordon, T. *J. Chem. Phys.* **2001**, *114*, 3065. (b) Iozzi, M. F.; Mennucci, B.; Tomasi, J.; Cammi, R. *J. Chem. Phys.* **2004**, *120*, 7029.
(20) Koeberg, M.; de Groot, M.; Verhoeven, J. W.; Lokan, N. R.; Shephard, M. J.; Paddon-Row, M. N. *J. Phys. Chem. A* **2001**, *105*, 3417.
(21) Read, I.; Napper, A.; Kaplan, R.; Zimmt, M. B.; Waldeck, D. H. *J. Am. Chem. Soc.* **1999**, *121*, 10976.
(22) The molecular solvation model requires several solvent parameters in the fit of eq 1, specifically:

	dipole moment (D)[a]	sigma (Å)[b]	polarizability (Å^3)	Lennard-Jones parameter (K)[e]	quad moment (D-Å)[a]
NMA	5.05	5.0	7.8[c]	304	9.54
NMP	4.29	5.4	8.0[d]	355	7.73

[a] MP2 (6-31G) Gaussian calculation. [b] Ben-Amotz, D.; Willis, K. G. *J. Phys. Chem.* **1993**, *97*, 7736. [c] *CRC handbook of chemistry and physics*, 75th ed.; CRC Press: New York, 1994. [d] Estimated by incrementing the volume and scaling to the NMA value. [e] Matyushov, D. V.; Schmid, R. *J. Chem. Phys.* **1996**, *104*, 8627.

$$\tau_{ET}^{*} = \sqrt{\frac{1}{\lambda_0 k_B T}}\frac{\exp(-\Delta G^{\ddagger}/k_B T)}{k_{ET}} \quad (6)$$

so that eqs 2 and 3 become

$$\tau_{ET}^{*} = \frac{\sqrt{\pi^3}}{\lambda_0 \sin\left(\pi\sqrt{\frac{\Delta G^{\ddagger}}{\lambda_0}}\right)}\tau_s + \sqrt{\frac{1}{\lambda_0 k_B T}}\frac{\exp(-\Delta G^{\ddagger}/k_B T)}{k_{NA}} \quad (7)$$

In the approximation that the first term in the sum over vibronic states in eq 1 dominates, the form of eq 1 is the same as the classical expression with an effective electronic coupling $|V_{eff}| = |V| \exp(-S/2)$ and eq 7 takes the form of a quasi-linear function of τ_s.

$$\tau_{ET}^{*} = \frac{\sqrt{\pi^3}}{\lambda_0 \sin\left(\pi\sqrt{\frac{\Delta G^{\ddagger}}{\lambda_0}}\right)}\tau_s + \sqrt{\frac{h}{2\sqrt{\pi^3}}}\frac{1}{|V_{eff}|^2} \quad (8)$$

This equation is not truly linear because of the temperature dependence of $\Delta_r G$ and λ_0 in the prefactor to τ_s; however, their net effect is virtually temperature independent over the range examined here, rendering eq 8 effectively a linear function of τ_s.

Figure 9B plots the value τ_{ET}^{*} of **1** in NMA and NMP versus the solvation time of NMA and NMP over the temperature range from 250 to 360 K. For large values of τ_s (>40 ps), a good linear correlation between τ_{ET}^{*} and the solvation time at low temperature is found. For smaller values of τ_s (see the inset), τ_{ET}^{*} is determined by the second term in eq 8, supporting the conclusion that the electron transfer is nonadiabatic at high temperature. The intercept from the fit to eq 8 (see Figure 9B) gives an electronic coupling $|V_{eff}|$ of 28 cm^{-1}. Using the values of $|V| = 146$ cm^{-1} and $S = 3.2$ (Table 2), $|V_{eff}| = 29$ cm^{-1}, in agreement with the value obtained from this analysis. However, Zusman's model overestimates the magnitude of the solvent effect observed here. The linear fit in Figure 9B has a slope of 0.09 eV^{-1}, which is 60 times smaller than the slope predicted from eq 8 (5.2 eV^{-1}). The behavior of **2** in NMA and NMP is similar to that of **1**, and the fit to eq 8 gives $|V_{eff}| = 11$ cm^{-1}, in good agreement with the value of $|V_{eff}| = 12$ cm^{-1}, calculated from $|V| = 62$ cm^{-1} used in the high-temperature analysis. The linear fit gives a slope of 0.68 eV^{-1}, which is 9 times smaller than the predicted slope, 6.4 eV^{-1}. Lastly, it is interesting to note that the difference between the low-temperature rates in NMA and NMP, which is apparent in Figures 4 and 8, is not evident in the plot versus the solvation time.

Zusman[8] derived a criterion to assess whether the dynamic solvent effect is manifest in an electron transfer reaction. In particular, if the inequality

$$\frac{\pi^2|V|^2\tau_s}{\hbar\lambda_0}\exp(-S) \gg \sin\left(\frac{\pi}{2}\left(\frac{\Delta_r G}{\lambda_0}+1\right)\right) \quad (9)$$

holds, then the solvent friction should be important. If the reaction occurs in the range of a small driving force, that is, $|\Delta_r G| \ll \lambda_0$, an effective electronic coupling can be defined as $|V_{eff}| = |V| \exp(-S/2)$. The dynamic solvent effect can be interpreted as an effective change of adiabaticity in the reaction, characterized by an adiabaticity parameter g

$$g = \frac{|V_{eff}|^2\pi^2\tau_s}{\hbar\lambda_0} \quad (10)$$

A g value less than 1 indicates an essentially nonadiabatic electron-transfer process, hence no dynamic solvent effect. By lowering the temperature, the solvation time can increase sufficiently to cause a crossover from nonadiabatic ($g < 1$) to a solvent friction controlled regime where $g \gg 1$. Using the parameters in Table 2, the dynamic solvent effect should manifest itself when $\tau_s \gg 7$ ps for **1** in NMA, $\tau_s \gg 35$ ps for **2** in NMA, $\tau_s \gg 6$ ps for **1** in NMP, and $\tau_s \gg 33$ ps for **2** in NMP. The fit to the experimental data predicts that $g \sim 1$ (i.e., $k_{SC} \sim k_{NA}$) for **1** in NMP when the solvation time is ~309 ps at 254 K and NMA is ~201 ps at 270 K. As with the analysis of the full eq 8, the transition ($g \sim 1$) occurs at a value of τ_s about 10 times larger than that predicted by Zusman.

The Zusman analysis provides a qualitatively consistent description for the rate constant over the entire temperature range. At high temperature, the solvation dynamics is fast, and the rate constant is limited by the electron tunneling step, that is, k_{NA}. At low temperature, the solvation is slow, and the electron transfer depends on the solvent friction. However, the predictions of this model do not *quantitatively* explain the experimental results.

Sumi−Marcus Model:[9,23] Electron transfer of **1** and **2** at high temperatures appears to lie in the fast diffusion limit, where the electron transfer is nonadiabatic. At lower temperatures, these molecules have $\lambda_v/\lambda_0 \sim 0.5$ and appear to lie closer to the narrow reaction window limit of Sumi and Marcus (see refs 6 and 9 for discussion of these limits). The reaction rate can be quantified by considering the average survival probability $Q(t)$ of the locally excited state. $Q(t)$ is the fraction of reactant molecules that have not transferred their electron by time t and is obtained directly from the fluorescence decay law. Sumi and Marcus consider both the correlation time $\tau_c = \int_0^\infty Q(t)dt$ and the average decay time $\bar{\tau} = 1/\tau_c \int_0^\infty tQ(t)dt$. These survival times provide valuable information about the time scale and temporal characteristic of the reaction rate. For example, if $\tau_c = \bar{\tau}$, then $Q(t)$ is a single-exponential decay, whereas $\tau_c \neq \bar{\tau}$ indicates a nonexponential decay law. Performing this analysis for the kinetics of **1** and **2** in NMA and NMP substantiates these conclusions and the manifestation of solvent friction effects.

Figure 10 plots $\tau_c\, k_{ET}$ (panel A) and $\bar{\tau}\, k_{ET}$ (panel B) as functions of $\tau_s k_{ET}$ in NMP and NMA. k_{ET} is extracted from the fit of the high-temperature data to the nonadiabatic model. $\bar{\tau}$ is calculated using a fit to a sum of exponentials.[24] If the reaction proceeded solely in the narrow reaction window limit, the slope of the log−log plot would be unity. However, for $0 < \lambda_v/\lambda_0 < 1$, the slope should lie between zero and unity.[23] In fact, the slope is less than 1, 0.58 in NMP and 0.72 in NMA (Figure 10A), which suggests that the reaction occurs close to the narrow reaction window limit. The fact that τ_c is different from $\bar{\tau}$ supports the interpretation that the reaction proceeds away from the fast diffusion limit. Comparison of the average survival times τ_c and $\bar{\tau}$ reveals that τ_c always deviates from $\bar{\tau}$ for **1** in NMA and NMP, the population decay is nonexponential and controlled

(23) Nadler, W.; Marcus, R. A. *J. Chem. Phys.* **1987**, *86*, 3906.
(24) $\bar{\tau} = \Sigma f_i \tau_i^2/\tau_c$, where f_i is the percentage of component i and τ_i is the decay time for component i, in a fit of the decay law to a sum of exponentials. τ_c is the correlation time.

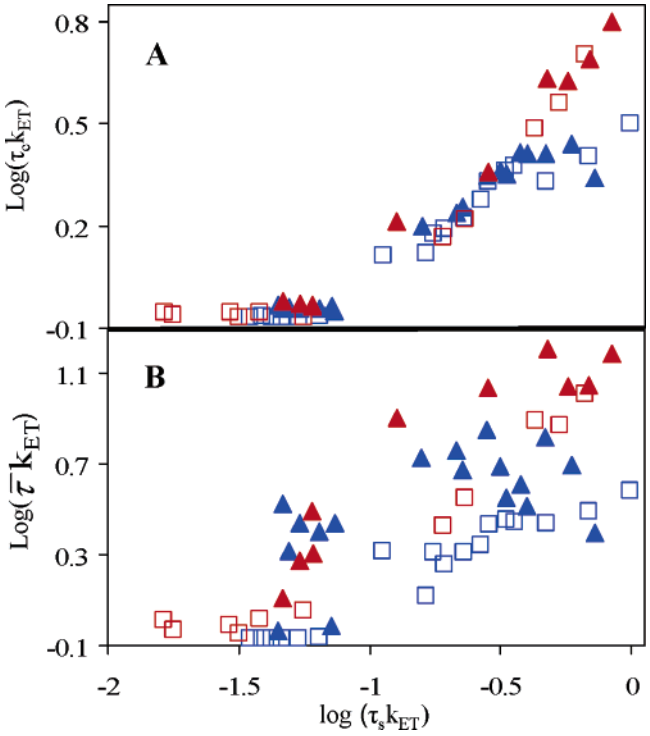

Figure 10. Plot of $\log(\tau_c k_{ET})$ (A) and $\log(\bar{\tau} k_{ET})$ (B) versus $\log \tau_s k_{ET}$ for **1** (filled triangle) and **2** (opened square) in NMA (red) and NMP (blue). k_{ET} is extracted from the fit of the high-temperature data to the nonadiabatic model.

by the solvent friction. In contrast, τ_c and $\bar{\tau}$ are similar for **2** in NMP, suggesting a single-exponential decay and a weak dynamic solvent effect. Figure 10 shows considerable noise for the $\bar{\tau}$ plot of **1**, so that the conclusions from it must be only qualitative. From Figure 10, it is evident that k_{SC} is smaller than the rate of solvation, $1/\tau_s$, and this occurs because of the activation energy, which also contributes to k_{SC}.

Discussion and Conclusion

The photoinduced intramolecular electron transfer in **1** and **2** display a dynamic solvent effect in NMA and NMP, even though the electronic coupling is small (see Table 2). By studying the rate constant over a large range of temperature, the electron-transfer mechanism can be followed from one in which the electronic coupling dominates the reaction to one in which the solvent friction controls the reaction. Since the electronic coupling is mediated by the pendant group, which is different in **1** and **2**, the change of fluorescence decay law from a single-exponential decay at high temperature to a nonexponential decay at low temperature occurs differently for these two molecules. The experimental rate constants differ for **1** and **2** at high temperature, but tend to be the same at low temperature. This trend is a consequence of the more sluggish solvation dynamics with decreasing temperature, as probed by dynamic Stokes shift experiments.

A curious feature revealed by both the electron transfer and the solvation dynamics measurements reported here is the qualitative similarity of the dynamics observed in NMA and NMP at low temperatures. This similarity is curious because neat NMA crystallizes below 303 K, whereas NMP remains liquid to 226 K. Most of the data in NMA were collected using polycrystalline samples. Clearly, both the solutes used for the solvation measurements and the electron-transfer molecules sense a local environment which is much more fluid than crystalline. Evidently, these "impurities" in the NMA solid exist in regions where the fluidity is similar to that in liquid NMP. These regions have reproducible properties that are comparable to what is expected for supercooled liquid NMA.

Because the solvation dynamics is relatively slow at low temperatures, experiments with different excitation energies were used to assess whether the locally excited state was equilibrated with the solvent. The rate constants do not change significantly with the excitation energy. This behavior confirms that when an electron transfers from the locally excited state to the charge-separated state the solute molecule retains no memory of the initial excess energy of the excitation.

Zusman's model for the effect of solvent friction on electron transfer was compared to the observations. The low-temperature rate constants correlate with the solvation rate, $1/\tau_s$, as determined through dynamic Stokes shift measurements. At high temperature, the rate constant is independent of τ_s. Quantitative comparison with the model gave an effective electronic coupling that is in good agreement with that found using eq 1 at high temperature (when high-frequency modes are included), and the adiabaticity parameter g, which can be defined from Zusman's criterion, predicts that the solvent friction limit applies. The plot of τ_{ET}^* versus the solvation time τ_s reveals a linear correlation at low temperatures; however, the slope does not match the theoretical prediction.

Three different possibilities can be identified for the discrepancy between the predictions of Zusman's model and the observed dependence of τ_{ET}^* on τ_s. One limitation of the Zusman description (eq 3) is the failure to explicitly include quantum modes in the reorganization energy. This possibility was noted earlier by Walker et al.,[25] who studied electron transfer in betaines and found that the theoretically predicted value was 10^6 times slower than their experimental value. In that case, the electron transfer proceeded in the inverted regime and quantum effects are expected to be critically important. They found that electron transfer in the slow solvent limit was controlled by vibrational motion. A second limitation of the Zusman treatment arises from the use of the high friction (Smoluchowski) limit for the solvent frictional coupling. Recently, Gladkikh et al.[26] extended Zusman's ideas to the intermediate friction regime and different barrier shapes. They found that the Zusman model overestimated the transfer rate by up to 10^3 and that the dynamics is a sensitive function of $|V|$ (or distance). A third limitation is the description of the solvation dynamics by a single relaxation time constant, whereas the solvation in these hydrogen bonding solvents is nonexponential. It may be that the faster components of the solvation response control the electron-transfer dynamics.[27,28] Although quantitative details of the Zusman description may be questioned, it appears to capture the physical picture of the process and approaches the correct nonadiabatic limit.

The electron transfer in **1** and **2** appears to lie in the narrow reaction window limit of the Sumi−Marcus treatment. Supporting this conclusion is the ratio of $\lambda_v/\lambda_0 \sim 0.5$ and the

(25) Walker, G. C.; Akesson, E.; Johnson, A. E.; Levinger, N. E.; Barbara, P. F. *J. Phys. Chem.* **1992**, *96*, 3728.
(26) Gladkikh, V.; Burshtein, A. I.; Rips, I. *J. Phys. Chem. A* **2005**, *109*, 4983.
(27) Hynes, J. T. *J. Phys. Chem.* **1986**, *90*, 3701.
(28) Fonseca, T. *Chem. Phys. Lett.* **1989**, *162*, 491.

nonexponentiality of the locally excited state's population decay. In this limit, the electron-transfer reaction occurs predominantly at a particular solvent polarization value, and the nonexponentiality arises from the time evolution of the reactant population along the solvation coordinate. The deviation of the correlation time τ_c and the average time $\bar{\tau}$ verifies the characteristics of the nonexponential decay law for the reaction. Other considerations of the Sumi−Marcus treatment, such as the electron-transfer rate being proportional to the solvation rate, are similar to the Zusman prediction. The important difference between the two models in this limit is that Sumi−Marcus predicts a nonexponential decay law, as observed, whereas the Zusman model does not address the issue.

By exploring the electron-transfer dynamics of two U-shaped molecules as a function of temperature in the slowly relaxing solvents NMA and NMP, the change in electron-transfer mechanism from a nonadiabatic reaction to a friction-controlled reaction is observed. Comparison to the theoretical model of Sumi−Marcus[9] shows that the decay law is nonexponential in the solvent friction limit. This study provides new insights into the factors governing the dynamics of electron transfer through nonbonded contacts.

Acknowledgment. N.I. and M.M. acknowledge support of The Office of Basic Energy Sciences, U.S. Department of Energy. M.P.R. acknowledges The Australian Research Council, The Australian Partnership for Advanced Computing (APAC), and The Australian Centre for Advanced Computing and Communications (ac3) for allocation of computing time. D.H.W. acknowledges support from the U.S. National Science Foundation (CHE-0415457) and thanks R. A. Butera for technical assistance.

Supporting Information Available: Additional experimental details and figures. This material is available free of charge via the Internet at http://pubs.acs.org.

JA055596A